

ChemComm

Accepted Manuscript



This is an *Accepted Manuscript*, which has been through the Royal Society of Chemistry peer review process and has been accepted for publication.

Accepted Manuscripts are published online shortly after acceptance, before technical editing, formatting and proof reading. Using this free service, authors can make their results available to the community, in citable form, before we publish the edited article. We will replace this *Accepted Manuscript* with the edited and formatted *Advance Article* as soon as it is available.

You can find more information about *Accepted Manuscripts* in the [Information for Authors](#).

Please note that technical editing may introduce minor changes to the text and/or graphics, which may alter content. The journal's standard [Terms & Conditions](#) and the [Ethical guidelines](#) still apply. In no event shall the Royal Society of Chemistry be held responsible for any errors or omissions in this *Accepted Manuscript* or any consequences arising from the use of any information it contains.

COMMUNICATION

Near Infrared-modulated Propulsion of Catalytic Janus Polymer Multilayer Capsule Motors

Cite this: DOI:
10.1039/x0xx00000x

Yingjie Wu, Tiejian Si, Xiankun Lin*, and Qiang He*

Received 00th January 2012,
Accepted 00th January 2012

DOI: 10.1039/x0xx00000x

www.rsc.org/

The use of a near-infrared (NIR) laser for reversible modulation of a bubble-driven Janus polymer capsule motor was demonstrated. This process was mediated through illumination of the metal face of the Janus capsule motor at the critical concentration of peroxide fuel. Such effective control of the propulsion of chemically powered microengines holds considerable promise for diverse applications.

The autonomous motion of chemically-powered artificial nano/micromachines has attracted a considerable recent interest, owing to their great promise for diverse future applications, such as nanoscale assembly and transport, microfactories, microactuators, drug delivery, nanoscale surgery, and motion-based biosensing.¹⁻³ Such challenging applications require new capabilities of chemically catalytic motors, including increased propulsion power, surface functionalization, precise motion control, surface functionalization, efficient cargo loading, transport and release.⁴⁻⁶ Particularly, a precise control of motion of such motors as well as the position and time that the motors work, is important for performing various tasks and diverse applications in future.⁷⁻¹⁰ Control of the directionality of chemically catalytic nano/micromotors has been commonly achieved by means of an external magnetic field or fuel concentration gradients.¹¹⁻¹⁶ Also, several strategies have been developed to regulate the speed of the motors, including application of thermal, electrical stimuli, ultraviolet or visible light.¹⁷⁻²⁰ Obviously, a physical input can be conveniently employed to turn on or off the motion in a wide range of environment at will. Moreover, light in the near-infrared (NIR) region is of special interest in the context of biomedical applications because bodily tissue has the highest transmissivity in this region (the so-called biological window).^{21, 22}

Here we demonstrate how the NIR-modulated “on/off” motion of a polymer multilayer capsule micromotor coated with a thin Platinum (Pt) shell can be achieved at a critical concentration region

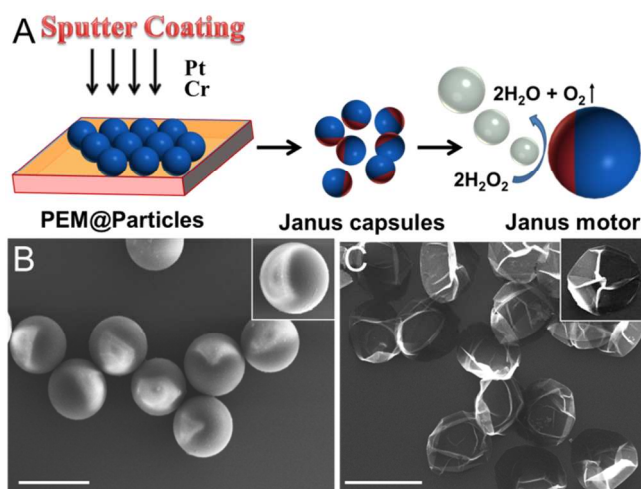


Figure 1. (A) Scheme of the synthetic procedure of Janus polymer multilayer capsule motors by using the layer-by-layer technique combined with a metal sputtering deposition method. (B, C) SEM images of Janus (PSS/PAH)₅ capsule motors before and after removal of the silica templates. Scale bar = 10 μm.

of a peroxide fuel (0.02% ~ 0.1%, v/v). Compared to other catalytic nanoengines, the capsules-based motors offer a large space for encapsulating therapeutic payload.²³⁻²⁷ In the previous studies, it has been found that with the decrease of fuel concentrations, the speed of chemically catalytic micromotors dramatically drop down, but can be enhanced with the increase of the solution temperature. In other words, the movement of such catalytic engines can be modulated by a small change in the localized temperature. The thin Pt shell plays two roles: a catalyst for the decomposition of peroxide fuel and a photothermal agent for heat generation. Upon NIR irradiation on the Pt face of a Janus capsule motor, the absorbed electromagnetic energy is dissipated as heat and thus forms a thermal

gradient along the direction from the Pt surface to the surrounding solution. This increased temperature gradient results in the accelerated kinetics of the catalytically chemical process, and the increased rates of mass transport. Therefore, the motion of Janus capsule motors could be modulated at will through a photothermal effect under a NIR laser illumination.

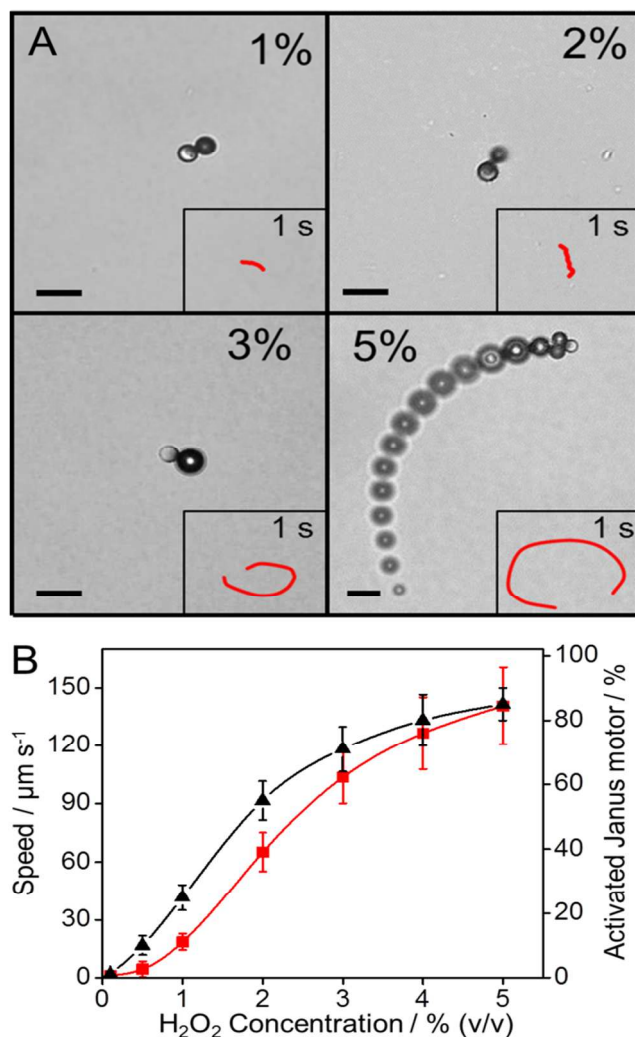


Figure 2. (A) The optical microscopic images of self-propulsion of Janus (PAH/PSS)₅ capsule motors in 1%, 2%, 3%, and 5% H₂O₂, respectively. The inset red curves represent the trajectories of Janus motors in 1 s. Scale bar = 10 μm . (B) Both the average speed (red curve) and the activated percentage (black curve) of catalytic Janus (PAH/PSS)₅ capsule motors change with the peroxide concentrations.

Janus polymer multilayer capsules were fabricated by a template-assisted layer-by-layer (LbL) method according to the procedures previously reported.²⁸⁻³¹ Briefly, five bilayers of negatively charged poly (styrene sulfonate) (PSS) and positively charged poly (allylamine hydrochloride) (PAH) were alternatively absorbed on the surface of 8 μm silica particles via the LbL assembly. Next, (PSS/PAH)₅-coated silica particles were deposited on a glass slide and then a 20 nm Pt layer was sputtered as illustrated in Figure 1A. Finally, Pt-modified Janus (PSS/PAH)₅ capsule motors were

obtained after the removal of the silica templates. Scanning electron microscopy (SEM) images in Figure 1B and C reveal the successful preparation of Janus (PSS/PAH)₅ capsule motors before and after removal of the silica templates. The diameter of (PSS/PAH)₅ capsule motors is approximately 8 μm corresponding to the used silica template size. For details of the deposition, characterization and NIR-irradiation methods, see SI. The brighter parts are ascribed to the deposit of the Pt component, and the surface area of the deposited Pt layers is roughly 40% ~ 50% of the total surface area of the capsule motors. The corresponding energy-dispersive X-ray (EDX) mapping analysis (SI Figure 1) displays the asymmetric distribution of Pt layers on Janus (PSS/PAH)₅ capsule motors. After the (PSS/PAH)₅ shells were labelled with a fluorescent isothiocyanate (FITC) dye, both fluorescence microscopy and confocal laser scanning microscopy images (SI Figure 2) show a green Janus structure, confirming the formation of Janus capsule motors and the stability of the assembled PSS/PAH multilayers.

As illustrated in Figure 2A, optical microscopy images, taken from ESI Video 1, show the bubble-driven movement of Janus (PAH/PSS)₅ capsule motors in hydrogen peroxide (H₂O₂) with concentrations of 1%, 2%, 3%, and 5%, respectively. One can see that all of oxygen bubbles were generated and subsequently released from that dark side (i.e. Pt layer), showing that Janus (PAH/PSS)₅ capsule motors are propelled unidirectionally by the generated oxygen bubbles. Also, a tail of oxygen bubbles could be observed at 5% H₂O₂, showing that the frequency of oxygen bubble release is higher than at other lower fuel concentrations. This means that the speed at 5% H₂O₂ is higher than others because the higher frequency of oxygen bubble release corresponds to the higher speed of Janus capsule motors. The inset red lines represent the tracking trajectories of Janus (PAH/PSS)₅ capsule motors in one second accordingly. One can see that the motor at 5% H₂O₂ could travel the longest distance compared with those of 1%, 2% and 3%, respectively. Furthermore, Figure 2B demonstrates that the speed of Janus (PAH/PSS)₅ capsule motors goes up with the increase of fuel concentrations. The average speed of the capsule motors increases from roughly 2 $\mu\text{m/s}$ at 0.5% H₂O₂ to the maximum speed of about 140 $\mu\text{m/s}$ at 5% H₂O₂ (18 body lengths/s) (Fig. 2B left y-axis, red line). It is found that with the decrease of peroxide fuel concentrations, the percentage of the activated catalytic micromotors dramatically drop from 85% at 5% H₂O₂ down to 10% at 0.5% H₂O₂ (Fig. 2B right y-axis, black line) accordingly. Obviously, all Janus (PAH/PSS)₅ capsule motors are almost motionless below 0.5% H₂O₂, which may be regarded as a critical fuel concentration region for effectively propelling Janus capsule motors.

Figure 3A shows that three Janus (PAH/PSS)₅ capsule motors remain motionless at 0.1% H₂O₂ in room temperature. In order to better understand the local photothermal effect on the “on/off” motion, two close Janus (PAH/PSS)₅ capsule motors were taken as a reference and a focused NIR laser at 808 nm with a power of 3 mW/ μm^2 was employed to illuminate that single capsule motor. The laser irradiation setup was home-made. We have described the setup in SI Figure 3. Before exposing to NIR laser, the Janus (PAH/PSS)₅ capsule motor stays in the “motion off” state. Once irradiated by NIR laser, the light-activated micromotor was accelerated within 0.3 s (a “motion on” state) and then reached to the maximum speed of

220 $\mu\text{m/s}$ compared to the referenced capsules as shown in Figure 3A and SI Video 2. It can be seen that once a NIR-activated microengine starts to move, it will leave the focused area of NIR laser and then the speed of the microengine gradually decreases to 0 $\mu\text{m/s}$ in 17 s. The NIR-activated movement of the Janus capsule motor is ascribed by the fact that NIR irradiation on the Pt side leads to the local increase of temperature surrounding the microengines because metals are known to dissipate heat upon light absorption. Therefore, the sharp increase of temperature rapidly induces higher rates of catalytic decomposition and mass transport, producing more bubbles and stronger propulsion force accordingly. The component of the bubbles was monitored by gas chromatography-mass spectrometry. The results indicate that the generated bubbles consist of oxygen, and no other gas components were detected (SI Figure 4). Moreover, the residual heat could still maintain a higher temperature so that the catalytic decomposition of peroxide fuel continues to occur even though the engine has left the laser spot.

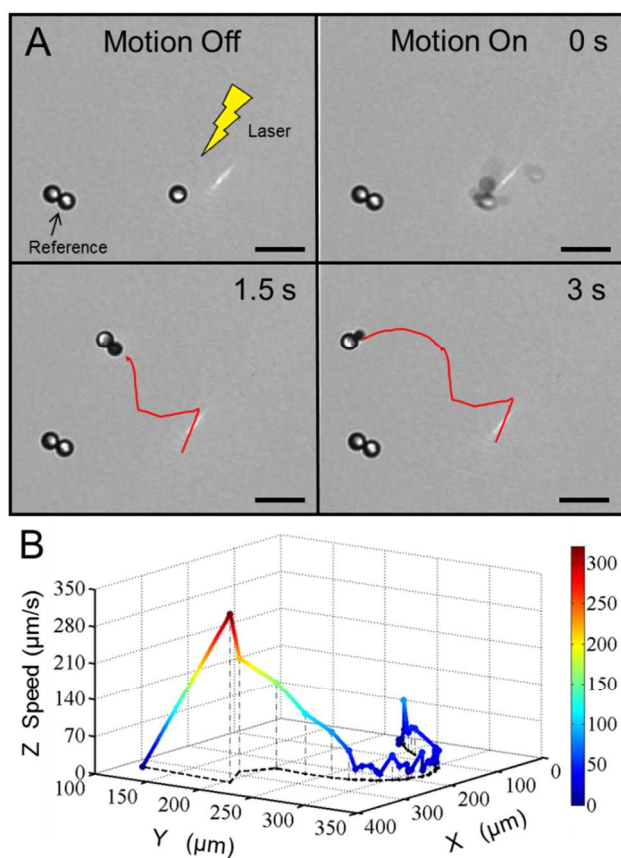


Figure 3. (A) The time-lapse optical microscopic images of the “switch on” motion of a Janus (PAH/PSS)₅ capsule motor under a focused NIR laser irradiation at 0.1% H₂O₂. The red line represents the tracking trajectory. (B) 3D profiles of the coloured curve corresponds to the trajectories (x, y) and the speed (z) of the motion in (A). Scale bar = 20 μm .

To better understand the photothermal effect of Janus capsule motors under NIR irradiation, we simulated the temperature change by using a heat diffusion equation that was used to study the thermoplasmonics modelling of Janus particles.³² When irradiation

with the NIR laser, the Janus motor creating local “hot spot” in the centre of the metal shell, the temperature soared by above 100 $^{\circ}\text{C}$ within less than one second. Due to the heat diffusion, a temperature gradient along the direction from the Pt surface to the surrounding solution is formed and the corresponding temperature profiles in Figure 4A have been obtained by solving the heat diffusion equation. According to our simulation, the rapid decay of temperature at the Pt/water interface also contributes to the initial acceleration due to the Soret effect. Compared to the bubble propulsion, however, this contribution could be neglected because the temperature difference is low and only lasts a short time in our study. In the control experiment, the start-up did not occur for the Janus motor in H₂O after NIR laser irradiation (SI Figure 5 and SI Video 4). This result suggests that the contribution of scattering and radiation pressure of the NIR laser or thermophoresis is also faint.

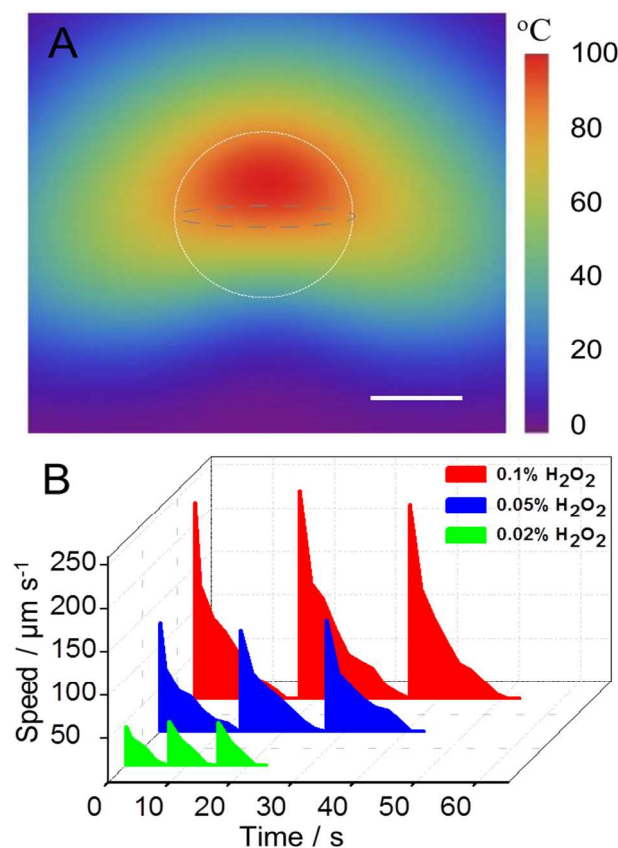


Figure 4. (A) Simulation of the photothermal effect of a micromotor. Elevated profile of temperature distribution on the vertical cross section of a Janus motor irradiated with a laser power of 3 $\text{mW}/\mu\text{m}^2$. Scale bar=5 μm . (B) Cyclic “On” and “Off” laser activation of the microengine motion. Data shown represent the average speed of motors in 0.02%, 0.05%, and 0.1% H₂O₂, respectively.

Reversibly stopping and starting the propulsion of catalytic Janus (PAH/PSS)₅ capsule motors should be performed by using this method. Figure 4B and corresponding SI Video 3 display the reversible “On/Off” switching of the motion of Janus (PAH/PSS)₅ capsule motors in peroxide fuel concentrations of 0.02% (a), 0.05% (b), and 0.1% (c), respectively. Similarly, Janus (PAH/PSS)₅ capsule

motors maintain motionless before switching on the laser. However, a sharp increase of the velocity is observed upon application of NIR illumination within 0.3 s. The maximum average speeds of the microengines are 45 ± 10 , 120 ± 20 , and 230 ± 30 $\mu\text{m/s}$ in the presence of 0.02%, 0.05%, and 0.1% H_2O_2 , respectively. When the capsule motors left the focused region of NIR laser which is regarded as switching off the NIR laser, the microengine motion stopped slowly in the 0.02%, 0.05%, and 0.1% H_2O_2 after 7, 13, and 17 s, respectively. These results further demonstrate that the maximum speeds of catalytic Janus capsule motors are also dependant on different fuel levels. Therefore, a wide range of micromotor speeds and run duration could be modulated through a combination of the fuel concentration and NIR illumination.

The rapidly starting artificial capsule motor is attributed to the accelerated kinetics of both the oxidation and reduction reactions of the peroxide fuel, and to a lower solution viscosity (and hence diminished resistance) with the rising local temperature. Under higher temperature, increasing molecular motion around the metallic shell also leads to the improved rates of mass transport, so the fuel consumption can supplement quickly. In this case, the photothermal effect caused by laser irradiation could lower the threshold of chemical fuel concentrations to propel Janus motors. When the motors moved out of laser-illuminated region, however, the photothermal effect disappeared. As a result, the temperature of the metal shell started to drop to room temperature and thus led to the deceleration of the micromotors.

In conclusion, we have demonstrated a novel approach for instantaneous activation of the motion of Janus catalytic motors by the remote NIR stimuli at the critical concentration of peroxide fuel. Such rapid and reversible motion control is attributed to the fact that a local sharp increase of temperature around the micromotors by a NIR-based photothermal effect results in the accelerated kinetics of redox processes and increased rates of mass transport. The "On/Off" switching of the motion of Janus capsule motors can be repeated many times by using an external "On/Off" NIR laser switch. The NIR-triggered speed modulation capability can be expanded to other types of chemically catalytic motors and thus paves the way to apply self-propelled synthetic engines in future.

This work was supported by the National Nature Science Foundation of China (91027045), and the Fundamental Research Funds for the Central Universities.

Notes and references

Key Lab for Microsystems and Microstructure Manufacturing, Micro/Nanotechnology Research Centre, Harbin Institute of Technology Yi Kuang Jie 2, Harbin 150080 (China)

E-mail: xiankunlin@hit.edu.cn; qianghe@hit.edu.cn

†Electronic supporting information (ESI) available: Related experimental protocols instrumentation, reagents, additional data and movies. See DOI: 10.1039/c000000x.

1. W. Gao and J. Wang, *ACS Nano*, 2014, **8**, 3170-3180.

2. Y. Mei, A. A. Solovev, S. Sanchez and O. G. Schmidt, *Chem. Soc. Rev.*, 2011, **40**, 2109-2119.
3. W. Gao, A. Pei and J. Wang, *ACS Nano*, 2012, **6**, 8432-8438.
4. F. Z. Mou, C. R. Chen, H. R. Ma, Y. X. Yin, Q. Z. Wu and J. G. Guan, *Angew. Chem. Int. Ed.*, 2013, **52**, 7208-7212.
5. R. F. Ismagilov, A. Schwartz, N. Bowden and G. M. Whitesides, *Angew. Chem. Int. Ed.*, 2002, **41**, 652-654.
6. M. Pumera, *Nanoscale*, 2010, **2**, 1643-1649.
7. J. Gibbs and Y. Zhao, *Frontiers of Materials Science*, 2011, **5**, 25-39.
8. J. Wang and K. M. Manesh, *Small*, 2010, **6**, 338-345.
9. S. Sanchez, A. N. Ananth, V. M. Fomin, M. Viehriig and O. G. Schmidt, *J. Am. Chem. Soc.*, 2011, **133**, 14860-14863.
10. Z. Wu, X. Lin, Y. Wu, T. Si, J. Sun and Q. He, *ACS Nano*, 2014, **8**, 6097-6105.
11. S. Balasubramanian, D. Kagan, K. M. Manesh, P. Calvo-Marzal, G. U. Flechsig and J. Wang, *Small*, 2009, **5**, 1569-1574.
12. M. Xuan, J. Shao, X. Lin, L. Dai and Q. He, *ChemPhysChem.*, 2014, **15**, 2255-2260.
13. D. A. Wilson, R. J. M. Nolte and J. C. M. van Hest, *Nat. Chem.*, 2012, **4**, 268-274.
14. V. Magdanz, G. Stoychev, L. Ionov, S. Sanchez and O. G. Schmidt, *Angew. Chem. Int. Ed.*, 2014, **53**, 2673-2677.
15. W. Gao, A. Pei, X. Feng, C. Hennessy and J. Wang, *J. Am. Chem. Soc.*, 2013, **135**, 998-1001.
16. Z. Wu, Y. Wu, W. He, X. Lin, J. Sun and Q. He, *Angew. Chem. Int. Ed.*, 2013, **52**, 7000-7003.
17. V. Yadav, H. Zhang, R. Pavlick and A. Sen, *J. Am. Chem. Soc.*, 2012, **134**, 15688-15691.
18. A. A. Solovev, E. J. Smith, C. C. BofBufon, S. Sanchez and O. G. Schmidt, *Angew. Chem. Int. Ed.*, 2011, **50**, 10875-10878.
19. T. Xu, F. Soto, W. Gao, V. Garcia-Gradilla, J. Li, X. Zhang and J. Wang, *J. Am. Chem. Soc.*, 2014, **136**, 8552-8555.
20. Z. Liu, J. Li, J. Wang, G. Huang, R. Liu and Y. Mei, *Nanoscale*, 2013, **5**, 1345-1352.
21. F. Z. Mou, C. R. Chen, Q. Zhong, Y. X. Yin, H. R. Ma and J. G. Guan, *ACS Appl. Mater. Inter.*, 2014, **6**, 9897-9903.
22. L. Xu, H. Kuang, C. Xu, W. Ma, L. Wang and N. A. Kotov, *J. Am. Chem. Soc.*, 2012, **134**, 1699-1709.
23. E. Donath, G. B. Sukhorukov, F. Caruso, S. A. Davis and H. Möhwald, *Angew. Chem. Int. Ed.*, 1998, **37**, 2201-2205.
24. M. Delcea, H. Mohwald and A. G. Skirtach, *Adv. Drug Deliver. Rev.*, 2011, **63**, 730-747.
25. J. Zhao, J. Fei, L. Gao, W. Cui, Y. Yang, A. Wang and J. Li, *Chem.Eur. J.*, 2013, **19**, 4548-4555.
26. K. Ariga, Y. M. Lvov, K. Kawakami, Q. Ji and J. P. Hill, *Adv. Drug Deliver. Rev.*, 2011, **63**, 762-771.
27. F. Caruso, *Chem-Eur. J.* 2000, **6**, 413-419.
28. X. Yan, J. Li and H. Mohwald, *Adv. Mater.*, 2012, **24**, 2663-2667.
29. D. Volodkin, A. Skirtach and H. Mohwald, *Polym. Int.*, 2012, **61**, 673-679.
30. Y. Wu, Z. Wu, X. Lin, Q. He and J. Li, *ACS Nano*, 2012, **6**, 10910-10916.
31. Y. Jia, Y. Cui, J. B. Fei, M. C. Du, L. R. Dai, J. B. Li and Y. Yang, *Adv. Funct. Mater.*, 2012, **22**, 1446-1453.
32. M. Z. Zhang, R.-N. Yu, J. Chen, Z.-Y. Ma and Y.-D. Zhao, *Nanotechnology*, 2012, **23**, 485104.